ADVANCED ENERGY MATERIALS
www.advenergymat.de

Optimized "Alloy-Parallel" Morphology of Ternary Organic Solar Cells

Zaiyu Wang, Yajie Zhang, Jianqi Zhang, Zhixiang Wei, and Wei Ma**

The emergence of organic solar cells (OSCs) has drawn much attention from both academy and industry due to their low cost for processing, easy synthesis, light weight, and flexibility nature.[1–7] Structure of OSC active layer has endured transition from initial bilayer planar heterojunction to bulk heterojunction (BHJ) to improve exciton dissociation efficiency. Further progresses in device performance have been achieved by the introduction of tandem cells to extend absorption range.[8,9] Although the power conversion efficiency (PCE) of tandem OSCs over 10% has been reported,[9–13] the complicated fabricating process becomes one of its drawbacks compared with ternary solar cells.[14,15] Ternary blend BHJ solar cell, which is made from the blends of two donors (D) and one acceptor (A) or two acceptors and one donor in order, is an alternative strategy to enlarge the absorption window.[14–21] As the fundamental device configuration of ternary blend BHJ is identical to the binary BHJ solar cell, the fabrication process of ternary BHJ is very simple.[17] In ternary blend solar cells, the polymer (D_1)/small molecule (SM, D_2)/fullerene (A) combination is especially interesting due to complementary properties on molecular aggregation,[22,23] phase separation,[23] and fabrication method. Benefiting from these advantages, the efficiency of the polymer/SM/fullerene ternary BHJ solar cell has been reported as high as 10.5%.[22]

Morphology is critically important to achieve high efficiency for ternary blend BHJ solar cells as keeping the efficient charge dissociation/transport/collection process as in the binary blend BHJ is the prerequisite to yield high performance. It is widely known that the crystallinity (or molecular packing), domain size, and domain purity of active layer play an important role for device performance in BHJ solar cells.[24–28] In ternary blends, these parameters are equally important but much more complicated because of the multiple phases at multilength scales. Well-ordered molecular packing is considered to be critical for charge transport and thus device performance.[29,30] However, for the most of cases, the mixture of two donor materials is deleterious for their individual molecular packing in ternary blends. For example, when the low bandgap polymer is introduced in the highly crystallized P3HT based binary blends, the ordered molecular packing of P3HT will be severely disrupted and thus the charge transport properties will be negatively impacted.[31] Also, in the high efficient PTB7 based ternary blend organic solar cells, the molecular packing in the ternary blend also becomes poorer compared to the referential binary blends.[32] Nevertheless, there has been no report showing that the introduction of the second conjugated donor component has helped with the crystallization of another conjugated donor materials and itself in ternary blends. On the other hand, the study of the phase separation behavior (domain size or domain purity) of individual components in ternary blends is difficult due to low contrast of different organic components. The case is even worse for the fullerene based ternary blend BHJ as the relatively high contrast between conjugated materials and fullerene will overcome the relatively weak contrast between different donor materials. Thus, the impact of domain size, average domain purity of the individual polymer-rich and SM-rich domains is still not clear in ternary blend organic solar cells.

Furthermore, the optoelectronics operation mechanism in ternary blend organic solar cells is also strongly morphology dependent. Two main models have been proposed in ternary blends. The "alloy" model (with the well mixed D_1/D_2 phases) proposed by Wei et al. and Street et al. suggests that the charges can be transported through "cascade" mode.[22,33] You and coworkers suggest a "parallel" model (with the distinguishable D_1/D_2 phase separation) in which ternary blends can be regarded as two independent binary subcells.[34] In reality, these two models can coexist by varying the compositional ratio of two donor materials and controlling the phase separation behavior. Furthermore, the vertical phase separation can also effectively impact the optoelectronics operation mechanism, for example, if the interface near to the anode/cathode is occupied by a higher/lower HOMO donor material in ternary blends, the holes/electron generated by the lower/higher HOMO materials will be trapped. However, due to the poor understanding of morphology in ternary organic solar cells, a systematic study of the operation mode in ternary blends as a function of the composition ratio and its impact on charge transfer mechanism has not been achieved.

In order to start addressing these outstanding questions, we used the polymer/SM/fullerene, i.e., PBDTTPD-HT/BDT-3T-CNCOO/$PC_{71}BM$ (chemical structures shown in **Scheme 1**a) ternary blends as a model system. This complements the recent report on the high device efficiency, for the time being, the same ternary system.[23] However, rather than seeking to optimize performance, we use the systems to elucidate complex morphology-performance relations. With the complimentary characterization tools, grazing incidence wide-angle X-ray scattering

Z. Wang, Prof. W. Ma
State Key Laboratory for Mechanical Behavior of Materials
Xi'an Jiaotong University
Xi'an 710049, P. R. China
E-mail: msewma@mail.xjtu.edu.cn
Dr. Y. Zhang, Dr. J. Zhang, Prof. Z. Wei
Key Laboratory of Nanosystem and Hierarchical Fabrication
National Center for Nanoscience and Technology
Beijing 100190, P. R. China
E-mail: weizx@nanoctr.cn

DOI: 10.1002/aenm.201502456

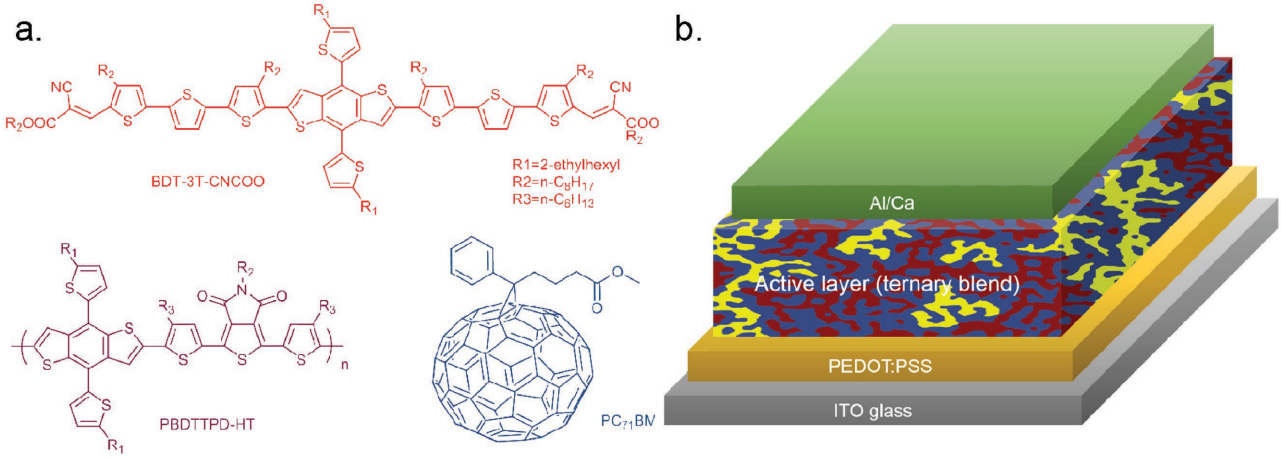

Scheme 1. a) Chemical structures of BDT-3T-CNCOO, PBDTTPD-HT, and $PC_{71}BM$. b) Device structure of ternary OSCs.

(GIWAXS) and resonant soft X-ray scattering (RSoXS), we find that, compared to the binary blend, the better face-on molecular packing for both polymer and SM is obtained. Meanwhile, for the first time, the individual polymer-rich and SM-rich domains can be distinguished and we find that the purer and reasonable small polymer and SM domains are achieved. Furthermore, we find that the vertical phase separation significantly impacts the charge transfer mechanism. Our studies support a morphology paradigm in actual devices in which enhanced molecular packing and optimized phase separation are critical in order to optimize performance, which can be achieved by carefully selecting a pair of SM and polymer. Based on the morphology investigation, our work also suggests that charge transfer mechanism is highly morphology dependent and a novel "alloy-parallel" model is proposed for ternary organic solar cells.

It has been previously reported that the crystallinity (π–π stacking) in ternary blends is enhanced compared to the binary blends, which leads to better charge carrier mobility and device performance.[23] Similar to the observation in the literature, the π–π stacking ordering is indeed improved at 40% as shown by GIWAXS (Figure S1, Supporting Information) in the ternary blend. It is considered that the improved molecular packing is achieved by the synergistic effect of polymer and SM. The presence of fullerene reduces this effect and adds the analysis complexity. Therefore, to rule out the role of fullerene and gain insight into the interaction between polymer and SM, and understand the origin of the enhanced crystallinity, the molecular packing and orientation of two donor materials blend is probed by GIWAXS. The GIWAXS profiles of two donor blends (BDT-3T-CNCOO: PBDTTPD-HT) with different SM ratios are shown in **Figure 1**a (the corresponding GIWAXS 2D patterns are shown in Figure S2, Supporting Information). For the pure PBDTTPD-HT thin film, only weak in-plane (100) peak at $q \approx 0.3$ Å^{-1} and broad out-of-plane (010) peak at $q \approx 1.65$ Å^{-1} are

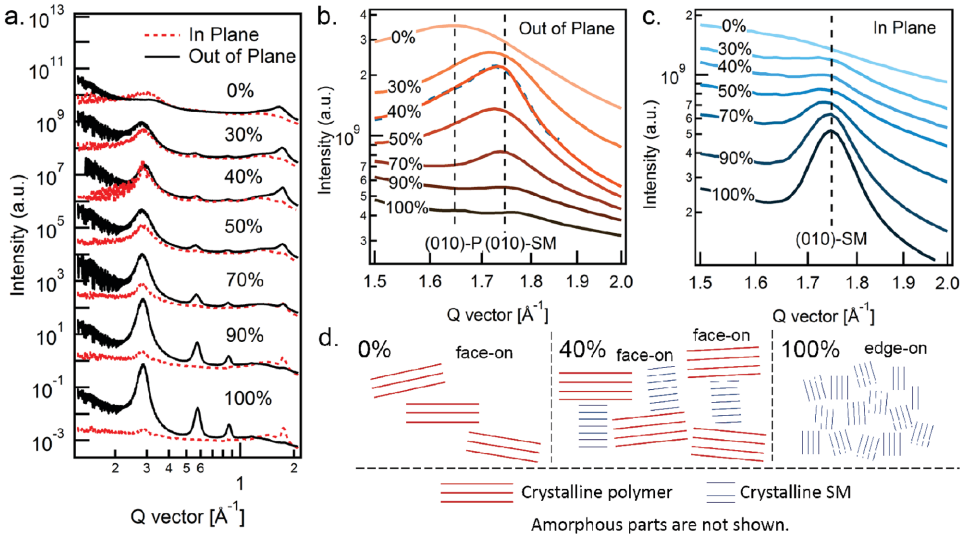

Figure 1. a) Out-of-plane and in-plane GIWAXS profiles of donor blends with different BDT-3T-CNCOO ratios. GIWAXS profiles are normalized by film thickness, penetration depth, and illuminated area. b,c) Enlarged view of b) out-of-plane, and c) in-plane π–π stacking (010) peak profiles. Dashed vertical lines are used to indicate peak location. Fitted scattering curve of 40% BDT-3T-CNCOO is also shown in dashed line. d) A sketch of changes of blend crystallinity with film composition variation.

observed, which indicates that PBDTTPD-HT shows the poor crystallinity and a preferential "face-on" orientation. For pure BDT-3T-CNCOO thin film, appearance of distinct out-of-plane (h00) peaking at $q \approx h \times 0.3$ Å^{-1} (h = 1, 2, 3) and in-plane (010) peaking at $q \approx 1.75$ Å^{-1} suggests that SM has better molecular packing than polymer and its preferential orientation is "edge-on". Due to the similar backbone and identical length of side chains, the location of lamella packing diffraction peaks for these two materials is identical, which increases the difficulty to distinguish their individual lamellar packing in the ternary blend. By gradually adding SM, out-of-plane (100) and in-plane (010) diffraction peaks vary in a monotonic mode, i.e., these peaks become less pronounced when amounts of SM decrease, demonstrating that the population of the overall "edge-on" molecules decreases as demonstrated in Figure 1c in detail. Furthermore, it is interesting to find that the intensity of in-plane (h00) and out-of-plane (010) peaks increases rapidly as the ratio of SM increases from 0% to 40% and then decreases gradually when the SM content exceeds 40%. This indicates that the "face-on" orientated molecule reaches the maximum at 40% in the ternary blend. It is further noted that although the difference of q location for peaks (h00) between PBDTTPD-HT and BDT-3T-CNCOO is so delicate that it is difficult to make quantitative analysis in depth as mentioned above, the disparity of π–π stacking (010) scattering peak location of two components, i.e., 1.65 Å^{-1} for PBDTTPD-HT and 1.75 Å^{-1} for BDT-3T-CNCOO (values from the corresponding pure films), allows us to distinguish their respective contributions. To emphasize this effect, Figure 1b,c displays the enlarged scattering profiles of (010) peak in the out-of-plane and in-plane direction for further analysis.

The development of the out-of-plane (010) peaks (shown in Figure 1b) varies in a nonmonotonic mode (i.e., pure PBDTTPD-HT and pure BDT-3T-CNCOO shows broad peaks but blend films exhibit sharper peaks) and the blend film with 40% BDT-3T-CNCOO shows the sharpest (010) peak. In order to quantitatively analyze this variation, we fit scattering profiles with multiple Gaussian functions (Figure S3, Supporting Information). Initially, we assume that the cocrystals are formed and only one π–π stacking peak is applied to fit the scattering data. However, the fitting is poor as demonstrated in Figure S3, Supporting Information. Then, the π–π stacking peaks (with q range from 1.6 to 1.9 Å^{-1}) are successfully fitted with two peaks, in which the location of two peaks corresponds to individual pure films ($q \approx 1.65$ Å^{-1} for PBDTTPD-HT; $q \approx 1.75$ Å^{-1} for BDT-3T-CNCOO). The peak with lower q (<1.5 Å^{-1}) represents the silicon substrate background. The fitted scattering curve of 40% BDT-3T-CNCOO blend film with double peaks is shown in **Figure 2**c as an example. The double π–π stacking peaks suggest that BDT-3T-CNCOO and PBDTTPD-HT molecules are not intercalated and both of BDT-3T-CNCOO and PBDTTPD-HT contribute to the "face-on" π–π stacking. The coherence length of the individual π–π stacking ordering was calculated using the full-width at half-maximum of the scattering peaks based on the Scherrer equation.[35] Coherence lengths of polymer along π–π stacking direction for 30%, 40%, and 50% SM ratio are 28, 47, and 21 Å, and meanwhile those for SM are 43, 93, and 45 Å, respectively. The out-of-plane π–π coherence length for polymer in binary blend (0% SM) is only 29 Å and no scattering peak

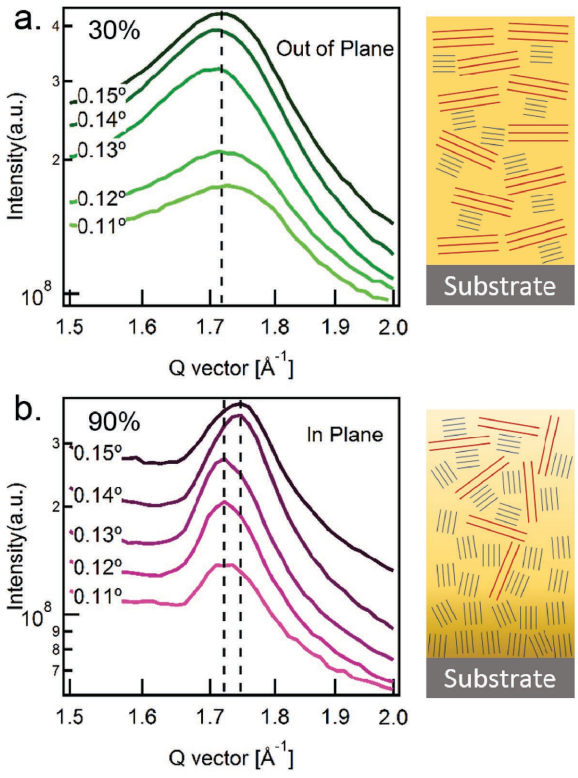

Figure 2. a) Out-of-plane GIWAXS profiles of 30% BDT-3T-CNCOO blend film. b) In-plane GIWAXS profiles of 90% BDT-3T-CNCOO blend film under different incident angles. Model diagrams on the right are used to show their respective film composition variation in vertical direction.

is observed for 100% SM in the out-of-plane direction. From the evolution of π–π stacking, we assume that the local "face-on" polymers induce more "face-on" SMs growing up along the π–π direction. Then, the enhanced "face-on" SM packing further leads to the longer polymer π–π packing. Thus, a synergistic crystallization effect was observed, and the "face-on" π–π stacking ordering is simultaneously improved for both polymer and SM when SM ratio is 40%.

The molecular packing variation in the vertical direction of blend films can be probed by varying the incident angle of GIWAXS. When the beam incident angle is smaller than the critical angle, only surface structure is probed. When the incident angle becomes larger, the beam can penetrate into the thin film and thus the bulk structure can be investigated. Higher incident angle leads to the deeper penetration. Out-of-plane (010) GIWAXS profiles of blend films with 30% SM and in-plane (010) profiles of 90% SM are shown in Figure 2a,b, respectively. The in-plane scattering selected for 90% SM is due to more fruitful information. For the blend film containing 30% SM, the location of (010) peaks remains almost unchanged as the incident angle varies, indicating that the blend film exhibits a uniform compositional distribution at different depths along vertical direction. However, for the 90% SM blend film, the location of (010) peaks has a conspicuous shift to higher q (near to $q \approx 1.75$ Å^{-1} corresponding to pure SM π–π stacking) at the incident angle of 0.14° and 0.15°. This variation suggests that there are more BDT-3T-CNCOO molecules aggregating around

the bottom of the blend than the surface of the blend (as indicated in Figure 2).Beyond the crystallinity of the two donor materials, RSoXS is performed to investigate phase separation of the ternary blend films on mesoscale and nanoscale, which has been shown to be critically important for photovoltaic performance.[26,27,36] Benefiting from the enhanced contrast and the compositional selectivity advantages, RSoXS is a perfect tool to investigate the complex phase separation of three-component system.[37] A photon energy of 284.2 eV was selected to provide high contrast between polymer, SM and fullerene, while decreasing mass-thickness contrast and avoiding high absorption above the absorption edges which can cause beam damage and fluorescence background.[26] The average scattering sector profiles of ternary blends with different weight fraction of SM are shown in **Figure 3**. It is interesting to note that the scattering can be fitted by multiple log-normal distributions and these multipeaks reflect a hierarchical morphology with phase separation at multiple length scales. When donors are only PBDTTPD-HT (0% SM), two evident peaks at $q \approx 0.03$ nm^{-1} and $q \approx 0.2$ nm^{-1} are observed, which indicates polymer: $PC_{71}BM$ phase separation on two length scales, which is consistent with transmission electron microscope (TEM) results as shown in Figure S4d, Supporting Information. For 100% SM blend film, the main peak at $q \approx 0.06$ nm^{-1} is attributed to the phase separation of SM and $PC_{71}BM$, and the shoulder on the right at $q \approx 0.15$ nm^{-1} is caused by the form factor. We estimate the phase separation length scale ξ of those referential binary blends using $\xi = 2\pi/q_{median}$. The length scale of 100 nm median domain spacing is found for SM: $PC_{71}BM$ blend, which is in accordance with the results gained from atomic force microscope (AFM) and TEM images (shown in Figure S4, Supporting Information). The phase separation of ternary blends with different component ratio is also investigated. Compared to the SM: $PC_{71}BM$ binary blend, the scattering profile of 70% SM entirely shifts to the higher q (smaller domains) without changing the shape. It is worth noting that no extra peaks are observed, which suggests that polymer chains are well mixed into the SM-rich matrix. Thus, the mixture of polymer and SM phases is formed when SM is the majority component. For the blend with 40% SM (polymer ratio reaching 60%), the scattering profile in the high q range is still similar to the SM: $PC_{71}BM$ binary blend but further moves to the higher q. Meanwhile, we find that a new peak emerges at $q \approx 0.06$ nm^{-1}, which is closed to the lower q in polymer: $PC_{71}BM$ binary blend and thus it is most likely originated from polymer: $PC_{71}BM$ phase separation. When the SM ratio decreases to 20%, the shape of the scattering profile in high q range is still closed to the scattering of SM-rich: $PC_{71}BM$. The polymer: $PC_{71}BM$ scattering peaks move to smaller $q \approx 0.04$ nm^{-1}. Overall, the presence of polymer leads to a reduced phase separation length scale for SM-rich: $PC_{71}BM$ in ternary blends. Also, the presence of SM reduces the phase separation of polymer: $PC_{71}BM$ in the ternary blend.

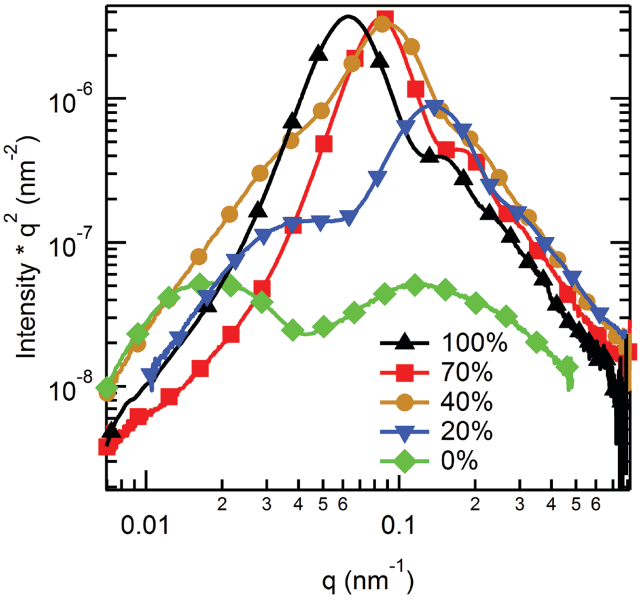

Figure 3. RSoXS profiles of donor blend films with different BDT-3T-CNCOO ratios.

The relative domain purity can also be evaluated by calculating the total scattering intensity through the integration of the scattering profiles over the q range and taking film thickness into account. It should be noted that the purity referred here is to describe the mixture degree of fullerene in polymer-rich or SM-rich phases, but not for the mixture of polymer and SM due to the low contrast. The overall average relative domain purities of 0.43, 0.71, 1, 0.88, and 0.69 are obtained for 0%, 20%, 40%, 70%, and 100% SM. It should be noted that purity of 40% SM set to 100% here is only for comparison convenience. The relative domain purity in ternary blends is higher than those in referential binary blends and 40% SM blend has the highest relative domain purity. If we consider the SM-rich: $PC_{71}BM$ and polymer-rich: $PC_{71}BM$ phase separation separately in the ternary blends, the relative purity of SM-rich: $PC_{71}BM$ is 0.87, 0.96, 1, and 0.89 for 100%, 70%, 40%, 20% SM and the relative purity of polymer-rich: $PC_{71}BM$ is 1, 0.37, and 0.21 for 40%, 20%, 0% SM. Therefore, the presence of SM induces the purer polymer-rich: $PC_{71}BM$ domains. Also, the presence of polymer induces the purer SM-rich: $PC_{71}BM$ domains. Overall, the relative domain purity analysis revealed that in ternary blends both polymer and SM domains are purified due to their synergistic effect, which is consistent with better molecular packing as revealed by GIWAXS in ternary blends.The following morphology diagram for ternary blends can be inferred from the above structural characterization. In molecular level, the GIWAXS shows that both SM and polymer exhibit enhanced "face-on" lamellar stacking and π–π stacking with respect to the electrode in ternary blends. The best "face-on" molecular packing is obtained at 40% SM. The "edge-on" molecular packing becomes less ordered when SM ratio decreases. The vertical compositional analysis by the angle-dependent GIWAXS shows that when the SM ratio is low (30%), the compositional distribution is homogenous, yet when SM ratio is high (90%), SM will enrich at the bottom of ternary blend films. In meso-length scale, the dominant phase separation is large for SM-rich: $PC_{71}BM$ and polymer-rich: $PC_{71}BM$ binary blends; adding polymers can reduce SM-rich: $PC_{71}BM$ domain size and adding SMs can reduce polymer-rich: $PC_{71}BM$ domains. When 40% SM is added, the domain size for both polymer- and SM-rich based domains is reasonably small and domains become

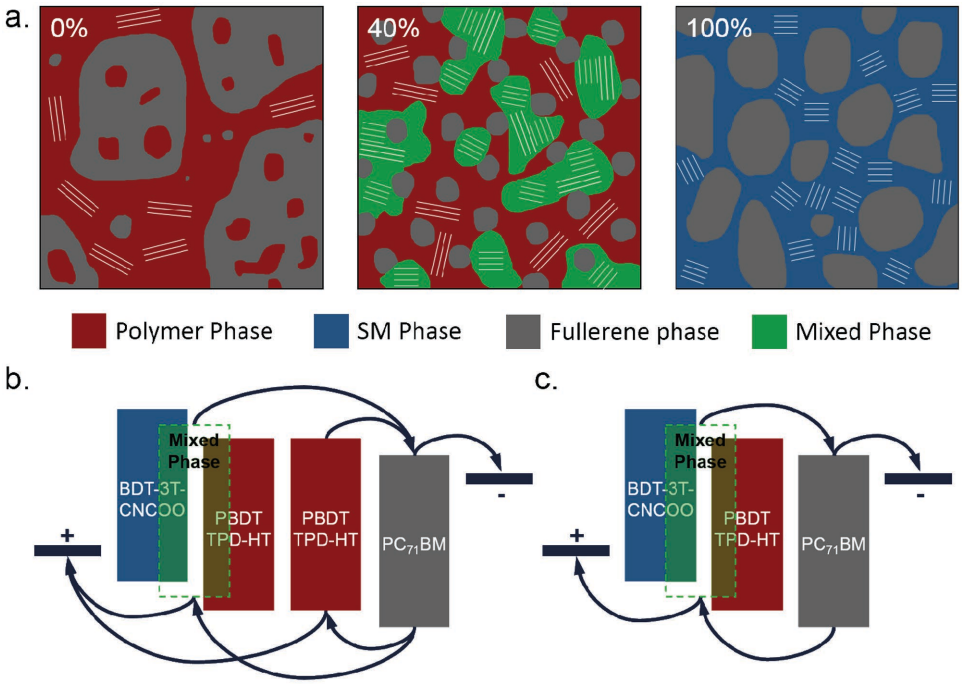

Figure 4. a) Morphology evolution with 0%, 40%, and 100% SM. b,c) Charge transfer mechanisms when SM is minority (b) and majority (c).

the purest (as shown in **Figure 4**a). When the polymer composition ratio is higher, polymer-rich: $PC_{71}BM$ phase separation occurs, and the device works as a mixture: polymer: fullerene ternary blend (as shown in Figure 4b). When the SM is the majority in the donor part, the SM and polymer are mixed and the device works as a mixture: fullerene binary blend (as shown in Figure 4c). Overall, the optimized molecular packing, domain purity (with fullerene), and domain size for both polymer-rich: $PC_{71}BM$ and SM-rich: $PC_{71}BM$ phases are achieved when 40% SM is loaded in the ternary blend.

By examining the device performance parameters based on ternary blends of OPVs, the enhancement of PCE compared to that of binary blends is mainly due to the improved fill factor (FF) and short-circuit current density (J_{sc}) (results shown in **Table 1**) at 40% SM. The improvement of J_{sc} in the ternary is due to two reasons: a) the ternary strategy enlarges absorption spectrum range as revealed by EQE results shown in Figure S5, Supporting Information, although the thickness of ternary blend is not the sum of the binary blends (83, 129, and 97 nm for 0%, 40%, and 100% SM); b) the dominant domain size for both polymer: fullerene and SM: fullerene is reduced in ternary blends. The smaller domain size to match exciton diffusion length at 10–20 nm is favorable for better charge dissociation efficiency.[38,39] Therefore, the improved absorption and charge dissociation efficiency leads to a higher J_{sc}.

The improved PCE is mainly due to the enhanced FF in the 40% SM ternary blend. The improvement of FF is related with charge transport property and charge carrier recombination.[40] Charge carrier (hole and electron) mobilities were measured using space charge limited current regime (Figure S6, Supporting Information). It is found that overall hole mobility is the bottleneck to achieve the balanced charge transport. The 40% SM ternary blend exhibits the highest hole mobility. It is considered that both polymer and SM show the best π–π stacking ordering at 40% in the ternary blend as revealed by GIWAXS, which leads to a better hole transport though π–π direction. Another factor to impact FF is bimolecular recombination. The light intensity study is carried out (shown in Figure S7, Supporting Information). The results show that the 40% ternary blend has less bimolecular recombination. This is mainly because the purer polymer and SM domains are archived at 40% SM. It is reported that pure domain shows a significant impact to reduce bimolecular recombination.[25] Therefore, we conclude that the improvement of FF originates from the improved π–π stacking ordering for both polymer and SM, and the purer polymer and SM based domains, which leads to the better charge transport property and less bimolecular recombination.The variation of open-circuit voltage (V_{oc}) in this ternary blend system is also interesting. We note that V_{oc} drops linearly as the SM composition increases, and becomes

Table 1. Summary of device performance and morphology parameters with 0%, 40%, and 100% ratio of BDT-3T-CNCOO.

SM ratio	PCE [%]	V_{oc} [V]	J_{sc} [mA cm^{-2}]	FF [%]	Poly.-Lπ–π [Å]	SM-Lπ–π [Å]	$\xi_{poly./full}$[nm]	$\xi_{SM/full}$ [nm]	Purity of poly./full	Purity of SM/full
0%	6.85	0.99	11.79	58.14	29	–	214	–	0.21	–
40%	8.40	0.98	12.17	71.23	47	94	80	70	1	1
100%	7.48	0.97	10.11	72.63	–	73	–	102	–	0.87

steady when the ratio of SM is greater than 40% (Figure S8, Supporting Information). It is highly possible that this distinct tendency is due to the evolution of morphology, which can be revealed by RSoXS and angle-dependent GIWAXS profiles. When the compositional ratio of SM is less than 40%, there is an evident phase separation between polymer and $PC_{71}BM$ as revealed by RSoXS and this phase separation disappears with an excess SM ratio over 40%. When the polymer: fullerene phase separation occurs, the cells work as parallel-like BHJ organic solar cells (mixed phase: polymer: fullerene), which is referred as a "alloy-parallel" model (shown in Figure 4b), and thus the V_{oc} varies as a function of the composition.[34] The steady V_{oc} pinned to the smaller V_{oc} of the corresponding binary blends can be partially accounted for by the absence of the polymer phase (mixed phase: fullerene, "alloy" model, shown in Figure 4c) and thus the corresponding channel for the hole transport. Another reason for steady V_{oc} is due to the compositional distribution along vertical direction. As revealed by the angle-dependent GIWAXS, SM enriches at the bottom of the ternary blend, which acts as the only hole transport layer, and thus V_{oc} is determined by the HOMO energy level of SM. Based on the V_{oc} variation and morphology paradigm, two different charge transfer mechanisms can be inferred in ternary blends as shown in Figure 4b,c. When the content of SM is less than 40%, holes can be transported independently in the mixed phase and polymer domains, which act as "alloy-parallel" cells. When the content of SM is more than 40%, all holes must pass through the SM-rich layer at the bottom of ternary blends before reaching to the anode.

In summary, we discussed for the first time the detailed relationship between device performance and morphology of the high performance polymer/SM/fullerene ternary solar cells, and a new "Alloy-Parallel" model for charge transfer and transport was proposed. We found that when the SM ratio was 40% in ternary blends, higher polymer "face-on" molecular packing, higher SM "face-on" molecular packing, purer polymer: $PC_{71}BM$ domains, purer SM: $PC_{71}BM$ domains, and optimized polymer: $PC_{71}BM$ and SM: $PC_{71}BM$ domain size, are simultaneously achieved. This favorable morphology leads to better charge transport mobility and less bimolecular recombination, which yields well-performed devices. More fundamentally, two different charge transfer mechanisms are revealed when the composition ratio is adjusted: (a) when the polymer ratio is high, the phase separation between polymers and SMs is occurred and devices work as "alloy-parallel" cells; (b) when SM ratio is high, SMs enrich at the bottom of ternary blends, which serves as the only hole transport layer. This study opens up a new frontier in understanding the critical structure-morphology-function relationship of polymer/SM/fullerene ternary blend devices, which can be used as a guide to design the other ternary blend solar cells.

Experimental Section

Grazing Incidence Wide-Angle X-ray Scattering Characterization: GIWAXS measurements were performed at beamline 7.3.3[41] at the Advanced Light Source (ALS). Samples were prepared on Si substrates using identical blend solutions as those used in devices. The 10 keV X-ray beam was incident at a grazing angle of 0.12°–0.16°, selected to maximize the scattering intensity from the samples. The scattered X-rays were detected using a Dectris Pilatus 2M photon counting detector.

Resonant Soft X-ray Scattering: RSoXS transmission measurements were performed at beamline 11.0.1.2[42] at the ALS. Samples for RSoXS measurements were prepared on a PSS-modified Si substrate under the same conditions as those used for device fabrication, and then transferred by floating in water to a 1.5 mm × 1.5 mm, 100 nm thick Si_3N_4 membrane supported by a 5 mm × 5 mm, 200 μm thick Si frame (Norcada Inc.). 2D scattering patterns were collected on an in-vacuum CCD camera (Princeton Instrument PI-MTE). The sample detector distance was calibrated from diffraction peaks of a triblock copolymer poly(isoprene-b-styrene-b-2-vinyl pyridine), which has a known spacing of 391 Å. The beam size at the sample is ≈100 μm by 200 μm. Samples used for RSoXS were prepared in the same way as for GIWAXS.

Device Fabrication: Patterned indium tin oxide (ITO) glass with a sheet resistance of 10 Ω sq^{-1} was purchased from CSG Holding Co., Ltd. (China). The ITO glass was cleaned by sequential ultrasonic treatment in detergent, deionized water, acetone, and isopropanol, and then treated in an ultraviolet-ozone chamber (Ultraviolet Ozone Cleaner, Jelight Company, USA) for 15 min. The blend of BDT-C83S-CNCOO:PBDTTPD-HT: $PC_{71}BM$ was dissolved in chloroform (CF) and spincoated on PEDOT:PSS modified ITO glass at 4000 rpm for 30 s. The prepared samples were annealed at 110 °C for 10 min before vacuum deposition of mental negative electrode. The active area of PSC is 0.04 cm^2. A typical film thickness of around 120 nm was obtained, which was detected by profilometer. Ca (20 nm) and Al (80 nm) cathodes were thermal evaporated in glove box at a chamber pressure of ≈4.0×10^{-6} Torr.

Supporting Information

Supporting Information is available from the Wiley Online Library or from the author.

Acknowledgements

The authors thank for the support from NSFC (21504006, 21534003, 51320105014). X-ray data were acquired at beamlines 7.3.3 and 11.0.1.2 at the Advanced Light Source, which is supported by the Director, Office of Science, Office of Basic Energy Sciences, of the U.S. Department of Energy under Contract No. DE-AC02-05CH11231.

Received: December 10, 2015
Revised: January 21, 2016
Published online:

[1] C. Deibel, V. Dyakonov, *J. Phys. Chem. Lett.* **2010**, *73*, 39.
[2] L. Dou, J. You, Z. Hong, Z. Xu, G. Li, R. A. Street, Y. Yang, *Adv. Mater.* **2013**, *25*, 6642.
[3] S. Gunes, H. Neugebauer, N. S. Sariciftci, *Chem. Rev.* **2007**, *107*, 1324.
[4] M. A. Green, K. Emery, Y. Hishikawa, W. Warta, E. D. Dunlop, *Prog. Photovoltaics* **2015**, *23*, 1.
[5] L. T. Dou, J. B. You, J. Yang, C. C. Chen, Y. J. He, S. Murase, T. Moriarty, K. Emery, G. Li, Y. Yang, *Nat. Photonics* **2012**, *6*, 180.
[6] G. Li, R. Zhu, Y. Yang, *Nat. Photonics* **2012**, *6*, 153.
[7] R. Søndergaard, M. Hösel, D. Angmo, T. T. Larsen-Olsen, F. C. Krebs, *Mater. Today* **2012**, *15*, 36.
[8] T. Ameri, N. Li, C. J. Brabec, *Energy Environ. Sci.* **2013**, *6*, 2390.
[9] J. You, L. Dou, K. Yoshimura, T. Kato, K. Ohya, T. Moriarty, K. Emery, C. C. Chen, J. Gao, G. Li, Y. Yang, *Nat. Commun.* **2013**, *4*, 1446.

[10] A. B. Yusoff, D. Kim, H. P. Kim, F. K. Shneider, W. J. da Silva, J. Jang, *Energy Environ. Sci.* **2015**, *8*, 303.
[11] J. You, C. C. Chen, Z. Hong, K. Yoshimura, K. Ohya, R. Xu, S. Ye, J. Gao, G. Li, Y. Yang, *Adv. Mater.* **2013**, *25*, 3973.
[12] C. C. Chen, W. H. Chang, K. Yoshimura, K. Ohya, J. You, J. Gao, Z. Hong, Y. Yang, *Adv. Mater.* **2014**, *26*, 5670.
[13] N. Li, C. J. Brabec, *Energy Environ. Sci.* **2015**, *8*, 2902.
[14] T. Ameri, P. Khoram, J. Min, C. J. Brabec, *Adv. Mater.* **2013**, *25*, 4245.
[15] P. P. Khlyabich, B. Burkhart, B. C. Thompson, *J. Am. Chem. Soc.* **2011**, *133*, 14534.
[16] Y. Yang, W. Chen, L. T. Dou, W. H. Chang, H. S. Duan, B. Bob, G. Li, Y. Yang, *Nat. Photonics* **2015**, *9*, 190.
[17] L. Y. Lu, M. A. Kelly, W. You, L. P. Yu, *Nat. Photonics* **2015**, *9*, 491.
[18] P. Cheng, X. W. Zhan, *Mater. Horizons* **2015**, *2*, 462.
[19] L. Yang, L. Yan, W. You, *J. Phys. Chem. Lett.* **2013**, *4*, 1802.
[20] B. M. Savoie, S. Dunaisky, T. J. Marks, M. A. Ratner, *Adv. Energy Mater.* **2015**, *5*, 6.
[21] T. Liu, L. Huo, X. Sun, B. Fan, Y. Cai, T. Kim, J. Y. Kim, H. Choi, Y. Sun, *Adv. Energy Mater.* **2015**, DOI: 10.1002/aenm.201502109.
[22] J. Zhang, Y. Zhang, J. Fang, K. Lu, Z. Wang, W. Ma, Z. Wei, *J. Am. Chem. Soc.* **2015**, *137*, 8176.
[23] Y. Zhang, D. Deng, K. Lu, J. Zhang, B. Xia, Y. Zhao, J. Fang, Z. Wei, *Adv. Mater.* **2015**, *27*, 1071.
[24] F. Liu, Y. Gu, J. W. Jung, W. H. Jo, T. P. Russell, *J. Polym. Sci. Pt. B: Polym. Phys.* **2012**, *50*, 1018.
[25] W. Ma, J. R. Tumbleston, M. Wang, E. Gann, F. Huang, H. Ade, *Adv. Energy Mater.* **2013**, *3*, 864.
[26] W. Ma, J. R. Tumbleston, L. Ye, C. Wang, J. Hou, H. Ade, *Adv. Mater.* **2014**, *26*, 4234.
[27] W. Ma, L. Ye, S. Q. Zhang, J. H. Hou, H. Ade, *J. Mater. Chem. C* **2013**, *1*, 5023.
[28] B. A. Collins, Z. Li, J. R. Tumbleston, E. Gann, C. R. McNeill, H. Ade, *Adv. Energy Mater.* **2013**, *3*, 65.
[29] J. R. Tumbleston, A. C. Stuart, E. Gann, W. You, H. Ade, *Adv. Funct. Mater.* **2013**, *23*, 3463.
[30] W. Li, S. Albrecht, L. Yang, S. Roland, J. R. Tumbleston, T. McAfee, L. Yan, M. A. Kelly, H. Ade, D. Neher, W. You, *J. Am. Chem. Soc.* **2014**, *136*, 15566.
[31] Y. Gu, C. Wang, F. Liu, J. H. Chen, O. E. Dyck, G. Duscher, T. P. Russell, *Energy Environ. Sci.* **2014**, *7*, 3782.
[32] L. Y. Lu, T. Xu, W. Chen, E. S. Landry, L. P. Yu, *Nat. Photonics* **2014**, *8*, 716.
[33] R. A. Street, D. Davies, P. P. Khlyabich, B. Burkhart, B. C. Thompson, *J. Am. Chem. Soc.* **2013**, *135*, 986.
[34] L. Yang, H. Zhou, S. C. Price, W. You, *J. Am. Chem. Soc.* **2012**, *134*, 5432.
[35] D.-M. Smilgies, *J. Appl. Crystallogr.* **2013**, *46*, 286.
[36] W. Ma, J. Reinspach, Y. Zhou, Y. Diao, T. McAfee, S. C. B. Mannsfeld, Z. A. Bao, H. Ade, *Adv. Funct. Mater.* **2015**, *25*, 3131.
[37] C. Wang, D. H. Lee, A. Hexemer, M. I. Kim, W. Zhao, H. Hasegawa, H. Ade, T. P. Russell, *Nano Lett.* **2011**, *11*, 3906.
[38] W. Chen, T. Xu, F. He, W. Wang, C. Wang, J. Strzalka, Y. Liu, J. Wen, D. J. Miller, J. Chen, K. Hong, L. Yu, S. B. Darling, *Nano Lett.* **2011**, *11*, 3707.
[39] W. Yin, M. Dadmun, *ACS Nano* **2011**, *5*, 4756.
[40] X. G. Guo, N. J. Zhou, S. J. Lou, J. Smith, D. B. Tice, J. W. Hennek, R. P. Ortiz, J. T. L. Navarrete, S. Y. Li, J. Strzalka, L. X. Chen, R. P. H. Chang, A. Facchetti, T. J. Marks, *Nat. Photonics* **2013**, *7*, 825.
[41] A. Hexemer, W. Bras, J. Glossinger, E. Schaible, E. Gann, R. Kirian, A. MacDowell, M. Church, B. Rude, H. Padmore, presented at *14th Int. Conf. Small-Angle Scattering (SAS09)*, Oxford, England, September 13–18, **2009**.
[42] E. Gann, A. T. Young, B. A. Collins, H. Yan, J. Nasiatka, H. A. Padmore, H. Ade, A. Hexemer, C. Wang, *Rev. Sci. Instrum.* **2012**, *83*, 045110.